Applied Nanoscience (2018) 8:1809–1821
https://doi.org/10.1007/s13204-018-0852-3

ORIGINAL ARTICLE

Bacillus lipopeptides: powerful capping and dispersing agents of silver nanoparticles

Vivek Rangarajan[1,2] · Gunaseelan Dhanarajan[1] · Pinaki Dey[3] · Dipankar Chattopadhya[4] · Ramkrishna Sen[1]

Received: 11 June 2018 / Accepted: 3 August 2018 / Published online: 9 August 2018

Abstract

This study demonstrates the use of *Bacillus* lipopeptides as both capping and stabilizing agents in the single-step synthesis of silver nanoparticles (Ag-NPs). With the aim to achieve a stable Ag-NP suspension, two methods of synthesis procedures, methods A and B, were tested and compared. In method A, the excess reactant sodium borohydride ($NaBH_4$) was added to the limiting reactant silver nitrate ($AgNO_3$), while in method B the limiting reactant was added to the excess reactant. It was found that, in both methods, the lipopeptide concentration significantly influenced the morphology and size of Ag-NPs. In case of method A, at low lipopeptide concentrations, Ag-NPs of uniform size distribution were synthesized, whereas at high concentration, incipient small nano-spheres of Ag-NPs were found concentrated at the vesicular surfaces during initial stage of reaction. However, at later stages, the smaller spherical particles radically changed into varied shapes and sizes and eventually detached from the vesicles completely. Ag-NPs of method B showed narrow size distribution. Stability studies revealed that Ag-NP suspension remained stable up to the sodium chloride, NaCl, concentration of 25 g/L. Steric and depletion types of stabilization were found to be the predominant mechanisms that imparted stability to the Ag-NPs. The particles were found to be stable up to test period of 6 months. Antimicrobial studies revealed that the lipopeptide-conjugated Ag-NPs with low lipopeptide were sensitive against all the tested organisms.

Keywords Lipopeptide · Silver nanoparticles · Capping agents · Nanoparticle stability · Antimicrobial activity

Introduction

Nanoparticles have unique properties that hold promising potential for applications in various fields of rapidly advancing science and technology. Metal nanoparticles, owing to their size/shape-dependent, unique, and tunable properties, e.g., quantum confinement (Rao et al. 2000), plasmon resonance (Hutter et al. 2001), and light scattering (Derkacs et al. 2008), find applications in wide areas such as electronics, optics, catalysis, and biotechnology (Du et al. 2018; Rao et al. 2000; Varade and Haraguchi 2012) By controlling the synthesis, it is possible to alter properties of nanosystems including surface area, optical and electrical properties, and the accessibility of the guest species.

Among the number of methods available for nanoparticle synthesis, liquid-phase methods such as forced hydrolysis, hydrothermal synthesis, sol–gel process, and reverse-microemulsion method have gained considerable attention from the commercial point of view, as they can generate many functional nanoparticulate materials with improved properties (Eastoe and Warne 1996; Goesmann and Feldmann 2010; Hanh et al. 2003; Liao et al. 2010). However, the most widely adopted is the chemical reduction method, in which the metal salts are converted to metal atoms using suitable reducing agents. A vast number of literature demonstrate the use of well-established protocols for the chemical synthesis of nanoparticles; there has been a growing interest in recent

Electronic supplementary material The online version of this article (https://doi.org/10.1007/s13204-018-0852-3) contains supplementary material, which is available to authorized users.

✉ Ramkrishna Sen
rksen@yahoo.com

[1] Department of Biotechnology, Indian Institute of Technology Kharagpur, Kharagpur, West Bengal 721302, India

[2] Department of Chemical Engineering, BITS Pilani, K.K. Birla, Goa Campus, Zuarinagar, Goa 403726, India

[3] Department of Biosciences and Technology, Karunya University, Coimbatore, Tamil Nadu 641114, India

[4] Department of Polymer Science and Technology, University of Calcutta, Calcutta, West Bengal, India

years for the use of biotechnological approaches as a cost-effective and scalable synthesis options (Kiran et al. 2010; Narayanan and Sakthivel 2010). Biotechnological-based approaches, in contrast to chemical synthesis method, do not require extreme processing conditions such as high temperature and pressure, and generally leave no toxic residues that may affect the environment.

The major concern in nanoparticle synthesis is tuning up these structures to obtain aggregates with desired morphology and properties. Capping agents play a very important role in determining the final quality of the particles (Raveendran et al. 2003). It essentially reduces the tendency of nanoparticles to agglomerate, by protecting the surface by either causing steric, electrostatic or depletion stabilization (Cushing et al. 2004). Besides, it serves as a diffusion barrier for further growth of nanoparticles (Gutiérrez-Wing et al. 2012). Compounds such as sodium dodecyl sulfate (SDS), cetrimonium bromide (CTAB), Triton X100, dioctyl sulfosuccinate (AOT), and polyvinyl pyrrolidone cap the nanoparticles by steric stabilization, while trisodium citrate caps by electrostatic stabilization forming a double layer over the metals (Chen and Hsieh 2002; Yonezawa et al. 2000) .

Biosurfactants owing to their superior properties such as biodegradability and micelle-forming ability (low Critical Micelle Concentration, CMC) are considered as green molecules. In nanoparticle synthesis, the use of biosurfactants as capping agents facilitates the uniform dispersion of the nanoparticles in the liquid medium. The studies involving the use of biosurfactants as dispersion agents were proven to be very effective for the uniform distribution of zirconia (Biswas and Raichur 2008) and colloidal alumina (Raichur 2007) nanoparticles by rhamnolipids, and cobalt nanoparticles (Kasture et al. 2007) by modified sophorolipids.

In the current study, the cross-flow ultrafiltration (CFUF)-purified lipopeptide was used as capping agent in the synthesis of silver nanoparticles (Ag-NPs) in the presence of sodium borohydride ($NaBH_4$) as reducing agent. Two synthesis approaches were adopted and compared. In the first approach, the reducing agent (excess reactant) was added to lipopeptide-stabilized $AgNO_3$ and in the second approach lipopeptide-stabilized $AgNO_3$ was added to the reducing agent. The nanoparticles synthesized were analyzed for their size, shape and stability, and further tested for their antimicrobial activities.

Materials and methods

Chemicals

Silver nitrate was purchased from Sigma Enterprises (US). Sodium borohydride was purchased from Merck, India. CFUF purified (Rangarajan et al. 2014) preparation as described elsewhere was used as capping agent. The composition of CFUF-purified lipopeptide used in the current study was 60:40% w/w of Surfactin:Fengycin.

Preparation of stock solutions

The stock solutions of $AgNO_3$ (20 mM) and $NaBH_4$ (100 mM) were prepared using MilliQ water. CFUF-purified lipopeptide stock was prepared in MilliQ water and the pH was adjusted to 8 using 1 M NaOH. All the stock solutions except $NaBH_4$ were prepared and stored in 4 °C until use. However, a fresh $NaBH_4$ stock was prepared for every experiment.

Preparation and characterization of lipopeptide solutions

The lipopeptide solution of required concentration was prepared by suitably diluting the stock solution in pH adjusted de-ionized water (pH = 8). The lipopeptide solutions were kept in bath ultrasonicator for 30 min, prior addition of the $AgNO_3$ or $NaBH_4$ into them.

The interactions between the lipopeptides micelles and Ag^+ ions were studied by observing the change in the surface tensions of the sample solutions.

The effect of Ag^+ ions on the size distribution of CFUF-purified lipopeptides was analyzed with the help of dynamic light scattering (DLS) analysis. Ag^+ concentration was maintained at 1 mM. The lipopeptide concentration was varied in terms of its CMC value; 25 mg L^{-1} (at CMC), 62.5 mg L^{-1} (2.5 times CMC) and 125 mg L^{-1} (5 times CMC).

Ag-NP synthesis using lipopeptide as capping agent

All synthesis reactions were carried out at 4 °C in a bath ultrasonicator. Two methods were adopted for the synthesis of Ag-NPs. The order and strategy of reactant addition, in addition to synthesis conditions, are important to obtain stable silver nanoparticles (Desai et al. 2012). Slow and drop-wise addition results in proper synthesis of nanoparticles. Similarly, the order of reactant addition, adding excess reactant to limiting reactant or limiting reactant to excess reactant, plays an important role in the synthesis of stable nanoparticles. For instance, the addition sequence can have significant effect of morphology and stability of nanoparticles, due to non-uniform mixing profiles and the subsequent change in the reaction kinetics.

Method A: addition of excess reactant (ER) into limiting reactant (LR)

In this method, $NaBH_4$ of 20 mM concentration was added drop by drop (@ 1 drop per second) to a

lipopeptide-capped $AgNO_3$ solution. $AgNO_3$ concentration was maintained constant at 1 mM, while the lipopeptide concentration was varied (25 mg L^{-1}, 62.5 mg L^{-1} and 125 mg L^{-1}). Both the reactants (ER and LR) were kept in separate bath sonicators maintained at 4 °C. The reactants were gently mixed with a glass rod, during the addition of $NaBH_4$. About 1 mL of sample was withdrawn for every 100 µL of $NaBH_4$ addition for further analysis.

Method B: addition of limiting reactant (LR) into excess reactant (ER)

In this conventionally method adopted, the lipopeptide-capped silver nitrate ($AgNO_3$ 1 mM in different lipopeptide solutions) was added drop by drop (@ 1 drop per second) to $NaBH_4$ solution. All other experimental conditions were maintained same as that discussed for the first method. The samples were withdrawn for every 1 mL addition of $AgNO_3$ solution.

Characterization of Ag-NP

UV–Vis analysis

UV–Vis absorption spectra of silver nanoparticles were measured by scanning the samples between the wavelengths 200 and 800 nm using Chemito double beam spectrophotometer. The samples were appropriately diluted before taking the absorption spectrum. For all the experiments, the sample solutions with $AgNO_3$ and lipopeptide, and without $NaBH_4$ were used as blank. The full width half maximum (FWHM) values of different spectra were calculated by approximating the data to Gaussian distribution using Originpro software (Version 8.0).

Transmission electron microscopy (TEM) analysis

The morphological features of the nanoparticles were analyzed by TEM (JEM–2100 HRTEM, Make–JEOL, Japan) with an acceleration voltage of 200 kV. Samples for TEM were prepared by placing a drop over the copper-coated copper grid. The energy-dispersive X-ray of nanoparticles was detected with an EDX detector (Oxford Instruments Analytical, England) equipped on the TEM. The average size and size distribution of the nanoparticle were calculated from TEM images using an open resource image processing software (ImageJ, US). The size distribution is reported in terms of number frequency in histograms (using originpro software).

Dynamic light scattering (DLS) analysis

The hydrodynamic diameter of lipopeptide micelles and synthesized nanoparticles were characterized using dynamic light scattering (DLS) analyzer, Malvern Zetasizer Nano ZS90 (Malvern Instruments Ltd., Worcestershire, UK), at 20 °C. The refractive index (RI) of the sample was found to be 1.330. The scattering angle was 173°. All the samples were measured in triplicates and values are expressed as averages. The measurement was taken for a total period of 60 S. All the samples were 0.22-µm filter sterilized before analysis. Zeta potential measurements of the samples were taken using the same instrument to test the stability of Ag-NPs as-synthesized by the two adopted methods as described earlier.

Fourier transform infrared (FT-IR) spectrometry

The samples were centrifuged at 15,000 rpm and the resulting lipopeptide-capped Ag-NP pellet was freeze dried. The lyophilized solid samples were used for analysis using FT-IR spectrometer (Model: Nexus-370, Thermo Nicolet Corporation, USA).

Stability studies

The stability of as-synthesized Ag-NPs was tested by varying the total salt concentrations. Sodium chloride (NaCl) was added to the Ag-NP suspensions prepared using method A to obtain different Ag-NP suspensions with NaCl concentrations of 0 g/L, 2 g/L, 5 g/L, 10 g/L, 25 g/L, 50 g/L and 75 g/L.

The stability studies were reported in terms of varying NaCl concentration, since the NaCl concentration was comparatively higher than other constituent ions concentrations such as Na^+ and NO^{3-}. In any case, the total concentration of unreacted salts did not exceed 0.52 g/L and was fairly constant.

Antimicrobial studies

Antimicrobial activities of lipopeptide-conjugated Ag-NPs were tested against two Gram-negative bacteria *E. coli* and *Proteus vulgaris*, and three Gram-positive bacteria, namely *Bacillus subtilis, Micrococcus flavus* and *Serratia marcescens*.

All the bacteria were grown in nutrient broth for about 6 h at 37 °C and about 50 µL of the grown cultures ($OD_{600} = 0.5$) were spread onto the Muller–Hinton agar (Himedia, India) plates using a glass spreader. About 30 µL of Ag-NP samples/controls were added to the wells made in agar.

Antibacterial activities of the samples were calculated based on the zone of inhibition (observation of clear zones around the wells).

Results and discussion

The UV–Vis spectra of naked Ag-NPs, without the presence of any stabilizing agent, are shown in Fig. 1. The spectrum showed wide surface plasma resonance (SPR) maxima at 416 nm. It also showed absorptions at longer wavelengths, indicating significant aggregation of Ag-NPs. The TEM image of the naked Ag-NPs (Fig. 2a) after a day showed aggregates of smaller sized particles, which further formed tree-like structure, similar to that of observation reported by (Baruwati et al. 2009) after 1 month of synthesis (Fig. 2b).

Effect of Ag^+ ions on lipopeptide micelle size distribution

An important aspect, which is believed to attribute to the strong capping potential of lipopeptide molecules during

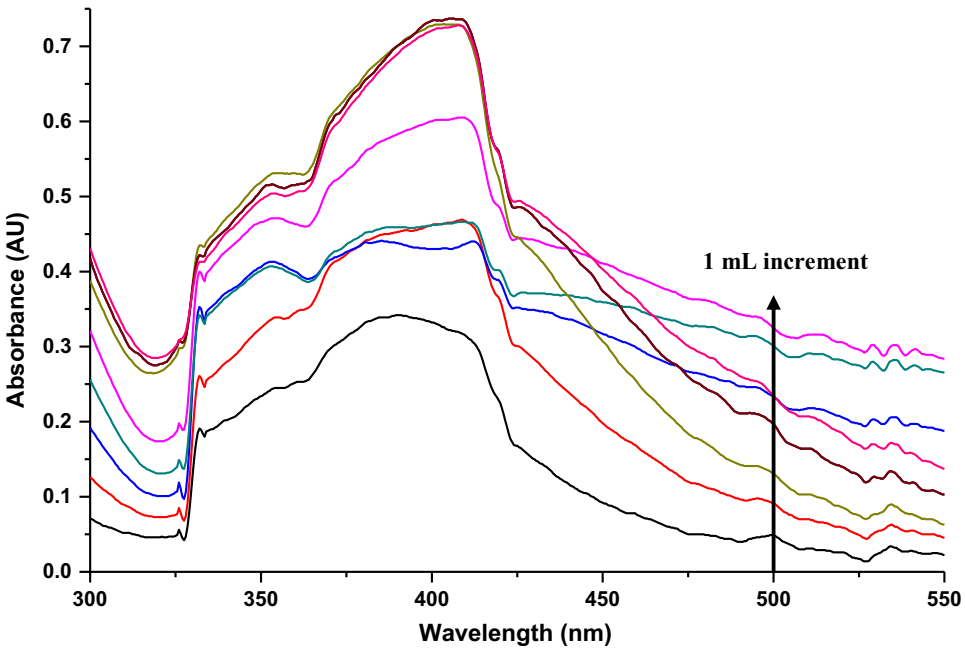

Fig. 1 UV–Vis spectra of naked Ag-NPs for every 1 mL addition of 1 mM $AgNO_3$ into 2 mM $NaBH_4$

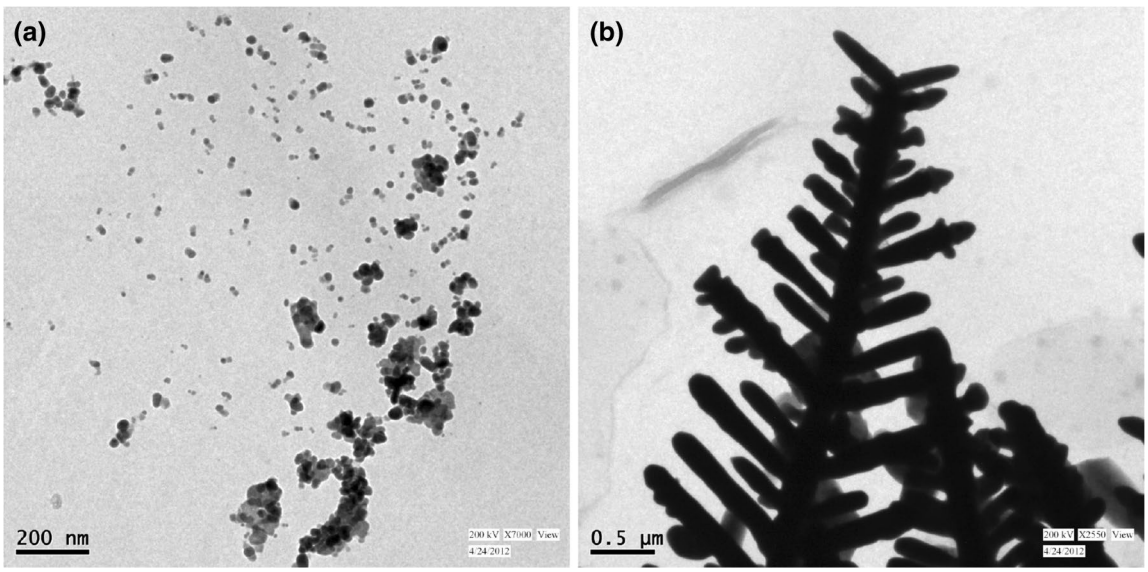

Fig. 2 TEM images of naked Ag-NPs (control) **a** after a day, **b** after 1 month of synthesis

nanoparticles synthesis, is their inherent ability to form supramolecular structures such as micelles and vesicles. However, the size of these supramolecular structures is mainly dependent on the concentration of surfactant molecules and the environment in which they are present. In particular, the type of cations present in the environment can significantly change the micelle structure. For instance, the anionic lipopeptide used in the current study has two carboxylate (COO^-) groups that can easily bind to divalent cations such as Mg^{2+}- and Ca^{2+}-forming bidentate (Rangarajan et al. 2014). The resultant minimization in electrostatic repulsion between lipopeptide monomers within the micelle facilitates packing of more monomers into the micelles, thereby increasing the stability of micelles. However, studies related to change in micelle sizes in the presence of larger sized Ag^+ ions and the resulting effect on the capping potential of lipopeptides have not been investigated before. So with the focus to achieve stable Ag-NP suspension, first, the change in the morphology of lipopeptide micelles in the presence of Ag^+ ions was investigated by measuring the change in surface tension and particle size distribution of micelles, before and after the addition of Ag^+ ions to the lipopeptide solution.

In contrast to our previous studies, wherein the divalent Ca^{2+} ions reduced the surface tension (Rangarajan and Sen 2013), the addition of monovalent Ag^+ ions (added as $AgNO_3$) at 1 mM concentration to the lipopeptide solution (25 mg L^{-1} at its CMC) increased the net surface tension of lipopeptide solution (Fig. 3). However, the initial reduction in surface tension at about 0.02 mM Ag^+ concentration could be attributed to the weaker interactions between the Ag^+ ions and peptide head groups. Furthermore, the DLS studies (Fig. 4a, b) revealed that the hydrodynamic radius of the micelles increased substantially in the presence of Ag^+ ions. The average hydrodynamic radius of lipopeptide micelles increased from 28.5 to 43.8 nm, when the lipopeptide concentration was increased from 25 to 125 mg L^{-1}. This indicated that though Ag^+ ions showed negligible influence on the CMC, it imparted significant changes to the conformation and size of the lipopeptide micelles. Based on these preliminary investigations, it could be hypothesized that the change in initial lipopeptide concentrations could strongly influence the morphological features and stability of Ag-NPs. The Ag-NP syntheses were studied at three different lipopeptide concentrations of 25 mg L^{-1}, 62.5 mg L^{-1} and 125 mg L^{-1}.

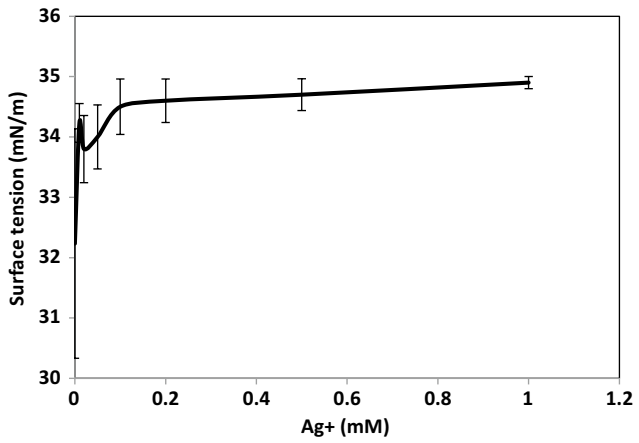

Fig. 3 Surface tension of lipopeptide solution, 25 mg L^{-1}, at different Ag^+ ion concentration

Characterization of as-synthesized AgNPs by two methods of preparation

UV–Vis spectroscopy

Method A In this method, Ag^+-containing lipopeptide solutions of three different lipopeptide concentrations (25 mg L^{-1}, 62.5 mg L^{-1} and 125 mg L^{-1}) were conditioned by maintaining them in bath ultrasonicator at 5 °C for 30 min. To maintain the structure of the micelles during Ag-NP synthesis, excess reactant at high concentration (20 mM) was added drop by drop into these solutions. The formation of silver nanoparticles was investigated by UV–

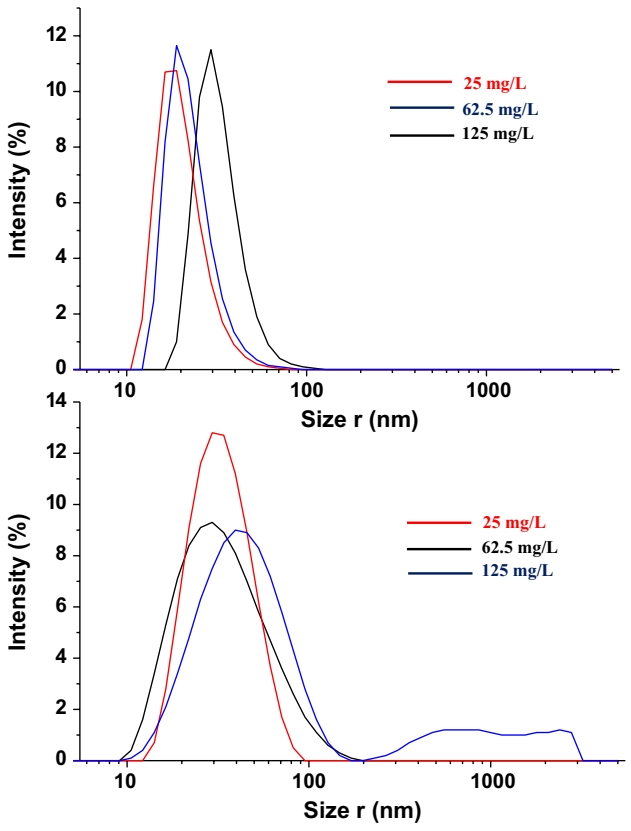

Fig. 4 Size distribution of micelles at different lipopeptide concentrations **a** without $AgNO_3$ and **b** in the presence of 1 mM $AgNO_3$

Vis spectrum of the sample solutions from the reaction mixture withdrawn after every 100 µL of $NaBH_4$ addition.

The disadvantage of this method was that Ag-NPs precipitated after few volume addition of excess reactant. In case of 25 mg L^{-1} lipopeptide solution, it occurred after 400 µL addition. However, precipitation occurred at later stages, 600 and 900 µL of $NaBH_4$ additions for lipopeptide concentrations of 62.5 and 125 mg L^{-1}, respectively.

Although the underlying mechanisms for the precipitation could not be elucidated, it could possibly be due to the gelling of lipopeptide–micelles induced by high localized concentration of $NaBH_4$.

Thus this micelle destabilization process promoted by the localized precipitation was found to be lipopeptide concentration dependent. From the UV–Vis spectra (Fig. 5a–c), it could be observed that surface plasmon resonance (SPR) position for different lipopeptide concentrations was found to be same and occurred invariably at about 417 nm, which is the characteristic feature indicating the presence of Ag-NPs. However, spectra were not observed to be of perfect Gaussian fit, which was suggestive of un-uniform particle size distribution.

The full width half maximum (FWHM), a parameter indicative of particle size distribution and sizes (White et al. 2012), increased with the increase in lipopeptide concentration. FWHM values calculated from the UV–Vis spectra of the sample solutions before the precipitation values were 138 and 164 nm for lipopeptide concentrations of 25 and 62.5 mg L^{-1}, respectively. For lipopeptide concentration of 125 mg L^{-1}, two new peaks emerged after 400 µL addition of $NaBH_4$. One was at lower wavelength of 372 nm and another at higher wavelength of 543 nm. In addition to these peaks, at later stages, after 500 µL addition, another peak appeared at 324 nm.

This manifestation of multiple SPRs indicated that Ag-NPs of different shapes and sizes might have been synthesized (Noguez 2007). However, better insight about the morphological features of Ag-NPs could be obtained only through TEM studies, which are discussed in later sections. Thus, the UV–Vis spectrum of Ag-NPs along with their respective FWHM values suggested that Ag-NPs of different shapes and sizes could be achieved by changing the concentration of lipopeptide.

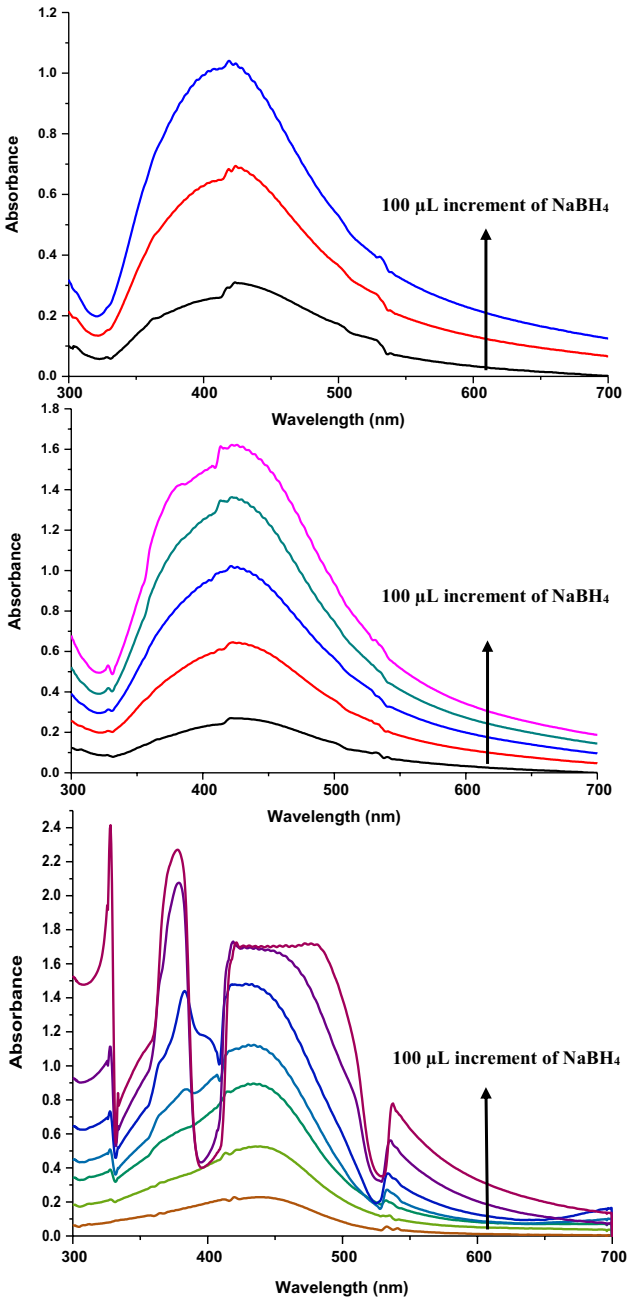

Fig. 5 UV–Vis spectra of Ag-NPs for every 100 µL addition of 20 mM $NaBH_4$ into 1 mM $AgNO_3$ at lipopeptide concentrations of **a** 25 mg L^{-1}, **b** 62.5 mg $L^{-1}$and **c** 125 mg L^{-1}

Method B In this method, the addition of limiting reactant ($AgNO_3$) to the excess reactant ($NaBH_4$) was expected to result in uniform dispersion of the synthesized Ag-NPs. These nanoparticles were expected to grow in numbers (seed particle generation) during the initial stage of $AgNO_3$ addition, which in later stage was expected to grow in size, due to continued addition of $AgNO_3$ to the reaction mixture. Such predictions were clearly reflected in the quality of the UV–Vis spectra and further in the TEM images as discussed later.

Unlike the UV–Vis spectra of Method A, the spectra of Method B were found to be of perfect Gaussian fits. The UV–Vis spectra for three different lipopeptide concentrations are given in Fig. 6a–c. No precipitations were observed immediately after synthesis for all the three tested concentrations of lipopeptide. The UV–Vis spectral scanning was conducted for the reaction mixtures after every 1 mL

(concentration = 1 mM) addition of $AgNO_3$. In all the three cases, the spectrum height increased during the successive addition of $AgNO_3$, which indicated increase in number of particles. However, no shift in SPR was observed. It was found to be same for different spectra of the same lipopeptide concentration.

The positions of SPR peaks at the end of the reaction were found to be 405.5 nm, 414 nm and 419.5 nm for lipopeptide concentrations 25 mg L^{-1}, 62.5 mg L^{-1} and 125 mg L^{-1}, respectively. The red shift to longer wavelengths (few nanometers variation) showed that the final size of Ag-NPs increased slightly with the increase in lipopeptide concentration. The spectrum broadened in size but decreased in height with the increase in lipopeptide concentration, indicative of increase in particle size distribution.

This was further corroborated by the increase in the FWHM values (99.2 nm at 25 mg L^{-1} to 121 nm at 125 mg L^{-1}) for these spectra with the increase in lipopeptide concentration.

However, the negligible change in FWHM values for different spectra (data not presented here), corresponding to the same lipopeptide concentration after every 1 mL addition of $AgNO_3$, showed that the particles grew only in numbers and not in sizes. The fact that the size of the particles was unaffected by the single-pot synthesis procedure adopted here validates the suitability of lipopeptide as capping agent in the synthesis of Ag-NPs with narrow size distribution.

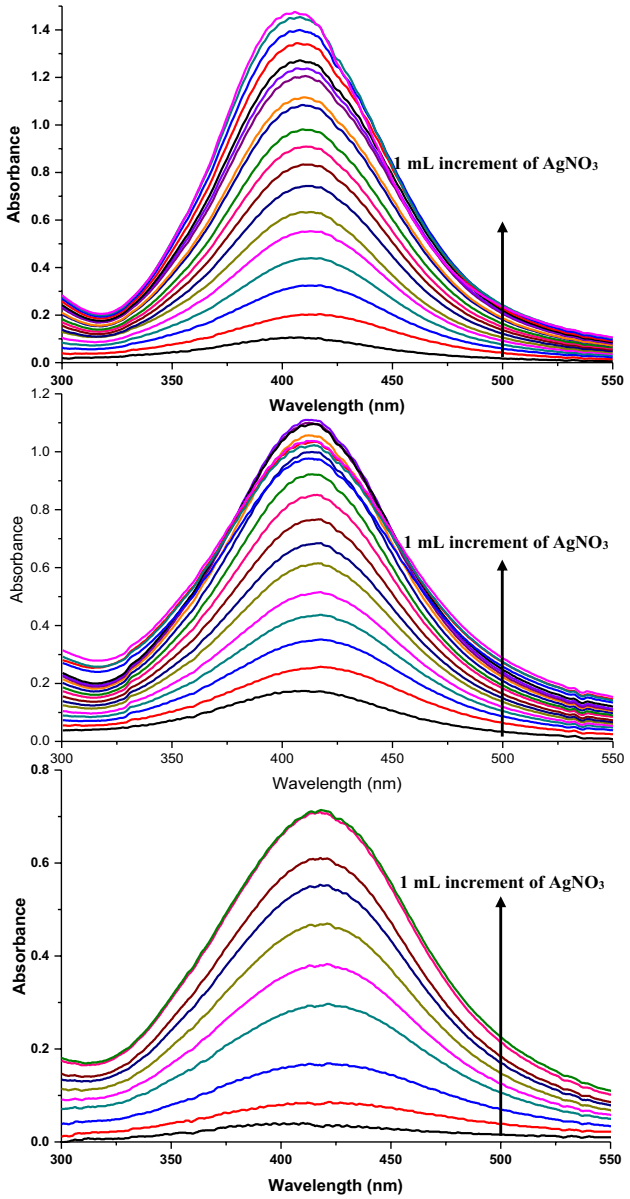

Fig. 6 UV–Vis spectra of Ag-NPs for every 1 mL addition of 1 mM $AgNO_3$ into 2 mM $NaBH_4$. at lipopeptide concentrations of **a** 25 mg L^{-1}, **b** 62.5 mg $L^{-1}$and **c** 125 mg L^{-1}

TEM studies

Method A

TEM analysis carried out for reaction mixtures before precipitation revealed many details about the morphology and the surrounding environment of Ag-NPs. The TEM images of the samples along with their selected area diffraction (SAD) patterns (inset of Figures) are given in Fig. 7a–c.

As predicted earlier from UV–Vis analysis, the size distribution of particles was found to be broader for all the lipopeptide concentrations used as shown in histograms (Fig. 7d–f). At lipopeptide concentration of 25 mg L^{-1} of, the average particle size was 11 ± 4.4 nm. The shape of the Ag-NPs was spherical. In the case of 62.5 mg L^{-1} lipopeptide, the Ag-NPs were seen along with micelles surrounded by them, which offered stability to these Ag-NPs as discussed later. The particles were found to be spherical in shape with wider size distribution and the average size of the particles was 22 ± 6.3 nm. For lipopeptide concentration of 125 mg L^{-1}, since the UV–Vis spectrum displayed unique patterns at different additions of $NaBH_4$, TEM analysis was performed for the reaction mixtures for every 100 µL of $NaBH_4$ addition. TEM image of sample after 100 µL $NaBH_4$ addition is shown in Fig. 7c. It could be observed that a few number of smaller sized incipient spherical nanoparticles were bound to the lipopeptide vesicles and the remaining unbound particles were seen suspended freely in the surrounding medium. At this high lipopeptide concentration, more than the expected numbers of Ag^+ ions were concentrated at the surface of micelles/vesicles through electrostatic interactions with the COO^- ions of amino acids. This concentrated Ag^+ at surface acted as reaction site (also called as stern layer) (Ewais 2014), which facilitated Ag-NP growth faster than in the surrounding medium. As described earlier, at this stage UV–Vis spectrum (Fig. 5c) revealed that there were no multiple peaks which were characteristic of

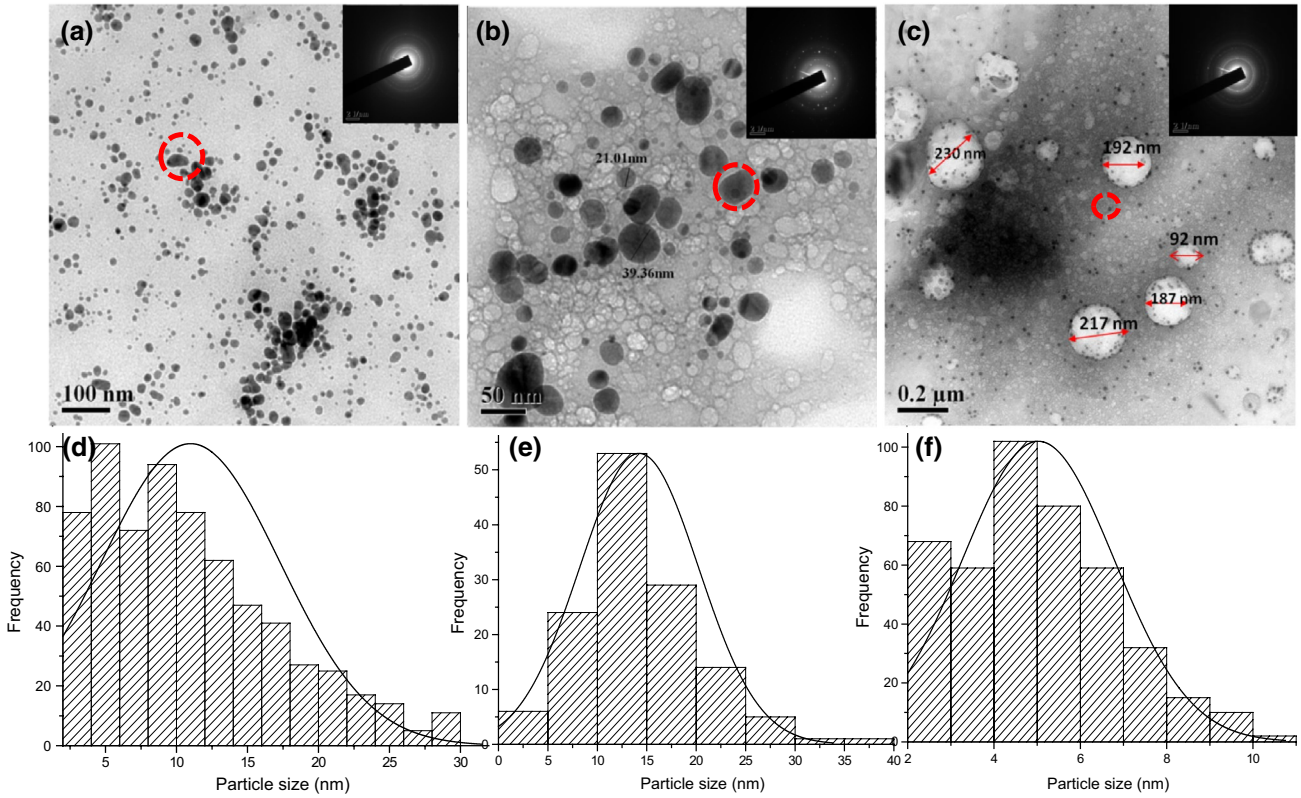

Fig. 7 TEM images of Ag-NPs prepared by method A at different lipopeptide concentrations **a** 25 mg L^{-1}, **b** 62.5 mg $L^{-1}$and **c** 125 mg L^{-1} and their corresponding histograms are given below from **d** to **f**. (The red circle indicates the area selected for SAD analysis)

multiple SPRs, due to smaller sized spherical particles. This observation of smaller NaP spheres bound to vesicular-like structures was similar to the works of Singh et al. (2014), which showed the attachment of Au-NPs to dehydrated vesicles at pH 10.

However, the size and shape of the Ag-NPs radically changed after successive additions of $NaBH_4$. TEM images of Ag-NPs after 300 and 600 µL additions are given in Supplementary Figures (A, B). It was observed that the particles not only grew in size but also found to be completely detached from the vesicles. In addition, the particles possessed different shapes (spherical, cylindrical, cubical, triangular, hexagonal, octahedral, tetrahedral, etc.) and sizes as shown in TEM images (Fig. 8). Thus, multiple SPRs were exhibited by Ag-NPs by the UV–Vis spectrum (Fig. 5c). The SAD patterns of the synthesized Ag-NPs revealed that particles were polycrystalline in nature. The presence of lipopeptide as the principal ingredient of vesicular structure was confirmed through the energy-dispersive X-ray (EDX) analysis of the vesicles (Supplementary Figure C), which showed only the presence of elements such as carbon and oxygen.

This transformation with respect to size and shape of the Ag-NPs and their subsequent effect on the vesicular structure may present us some interesting applications. For instance, vesicle-bound Ag-NPs may find application in controlled drug delivery. As the idea presented here is rudimentary, exhaustive works have to be carried out before the practical application of such application is realized. TEM analysis of the samples revealed that both the shape and size of the particles could be controlled by changing the concentration of the capping agent, lipopeptide.

Although the size distribution of Ag-NPs was wider, the particles were found to be more stable than the particles synthesized through method B as discussed later in the stability studies.

Method B

TEM analysis of the samples given in Fig. 9a–c showed the presence of individual and nearly spherical Ag-NPs without any aggregation. Histograms of the particles (Fig. 9d, e) showed narrow size distribution of Ag-NPs synthesized for lipopeptide concentrations of 25 and 62.5 mg L^{-1}. However, the size distribution of Ag-NPs was slightly broader (Fig. 9f) for 125 mg/L lipopeptide concentration. This trend could be attributed to the fact that a few number of Ag-NPs bound to vesicles were larger in size, when compared to freely suspended NPs. The

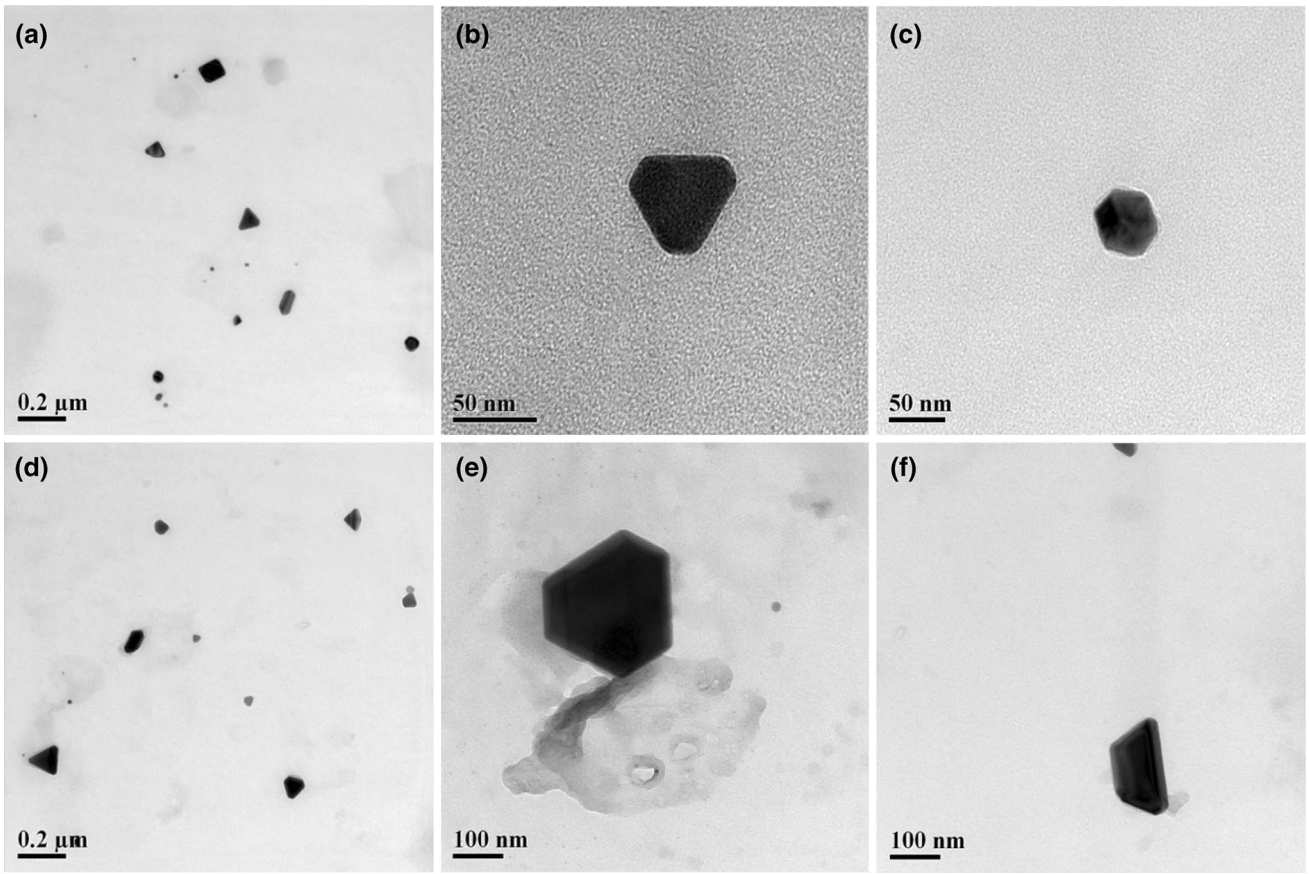

Fig. 8 Nanoparticles of different morphologies produced by method A at lipopeptide concentration of 125 mg L^{-1} after 700 µL addition of reducing agent

ability of micelles/vesicles to increase the rate of metal ion reduction by concentrating the metal ions on to their surfaces might have resulted in formation of larger particles at micelle–liquid interphase. Furthermore, the binding of Ag-NPs to the surface of micelles/vesicles facilitated synthesis of Ag-NPs of different morphologies. Although, this concept can be extended to both methods of synthesis, the vesicles of method B were not as stable as that of Method A, due to the progressive dilution of the reaction mixture during synthesis. This, in turn, affected the stability of the lipopeptide-conjugated Ag-NP suspension as discussed later in the stability studies. From the TEM analysis, it could be concluded that Ag-NPs of uniform size distribution with nearly spherical shapes were obtained for low lipopeptide concentrations. The varied-shaped particles showed the size-directing ability of micelles at high lipopeptide concentrations. The SAD patterns of different samples showed that Ag-NPs were polycrystalline in nature and the average size of the Ag-NPs for lipopeptide concentrations 25 mg L^{-1}, 62.5 mg L^{-1} and 125 mg L^{-1} were found to be 16.7 ± 1.2 nm, 22.14 ± 1.5 nm and 22.25 ± 4.5 nm, respectively.

Stability studies

The lipopeptide used in this study was intended to serve dual as both a capping agent during NP synthesis, and as a stabilizing agent post the synthesis. The role of lipopeptide as capping agent during synthesis at different initial concentrations has already been demonstrated. It has been well established that the stabilizing agents render stability to the colloids by one or combination of the mechanisms, namely steric, electrostatic or depletion stabilization (Xing et al. 2012). So, it is imperative to understand the stabilization mechanism which is predominant in the case of lipopeptide. The Ag-NPs synthesized from method A are given in Fig. 10.

Stability of the Ag-NPs was studied by different methods to ascertain the mechanism of stabilization. In the first method, the Zeta potential of different colloidal suspensions was measured. A higher zeta potential indicated greater electrostatic repulsion between the particles which in turn effectively prevented the agglomeration of particles (Pattekari et al. 2011). The anionic lipopeptide used in the current study imparted net negative charge to Ag-NPs by

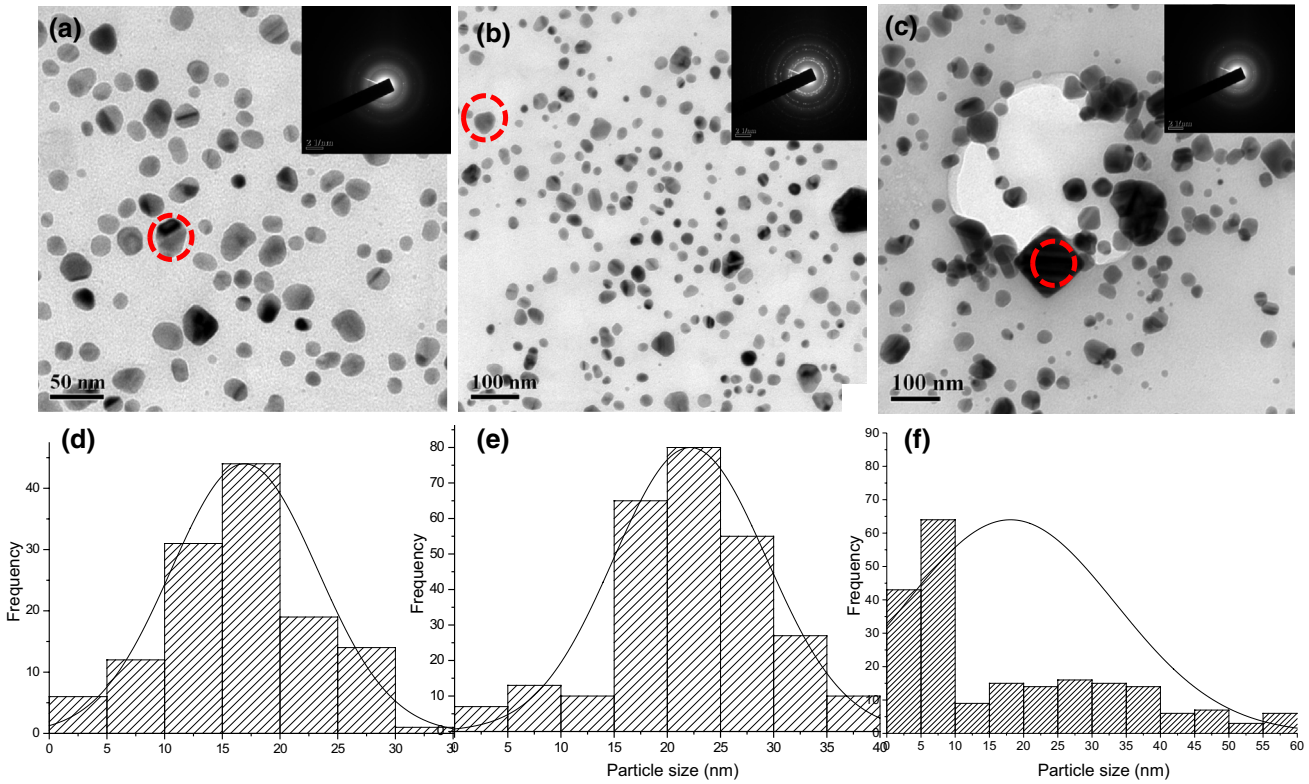

Fig. 9 TEM images of Ag-NPs prepared by method B at different lipopeptide concentrations **a** 25 mg L^{-1}, **b** 62.5 mg L^{-1} and **c** 125 mg L^{-1} and their corresponding histograms are given below from **d** to **f**. (The red circle indicates the area selected for SAD analysis)

Fig. 10 Laser light path traversing through Ag-NPs colloids

forming electrical double layer at low lipopeptide concentrations (Chaudhari et al. 2007) or by forming supramolecular structures such as micelles/vesicles for moderate to high lipopeptide concentrations.

Table 1 Average particle size and zeta potential values of Ag-NPs of method A and B at different lipopeptide concentrations

Sample	Zeta potential (mV), [Avg particle size (nm)]		
	25 mg L^{-1}	62.5 mg L^{-1}	125 mg L^{-1}
Method 1	− 34.8, [10.99]	− 53.2, [16.33]	− 44.5, [4.83]
Method 2	− 22.2, [16.9]	− 28.7, [22.14]	− 46.2, [22.25]

The Zeta potential of the different samples (Table 1) indicated that, in general, the Ag-NP suspensions obtained by both methods were found to be stable. However, Ag-NPs of Method A showed comparatively higher stability than of method B. This was corroborated by the presence of little precipitates in all samples of Method B after 2 months.

To elucidate the underlying mechanism that imparted stability to Ag-NPs, the UV–Vis spectra of different samples of method A (lipopeptide concentration = 62.5 mg L^{-1}) at different amounts NaCl were compared (Fig. 11). It was observed that the height of the spectrum gradually dropped until the NaCl concentration of 25 g L^{-1}. The addition of NaCl at low amounts caused no significant change in the OD_{max} as well as the SPR of the spectra. However, the spectrum height decreased significantly for NaCl concentrations beyond 50 g L^{-1},

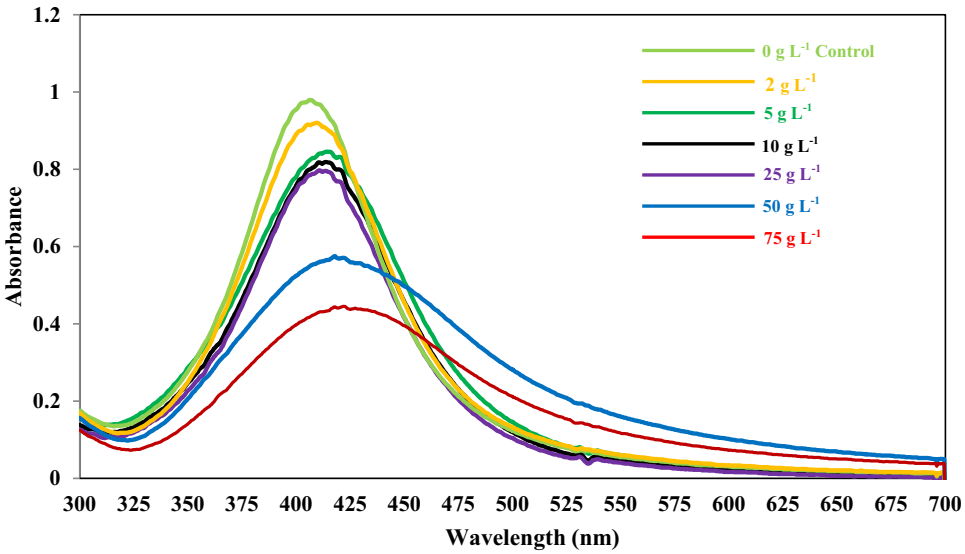

Fig. 11 UV–Vis spectra of Ag-NPs solutions at different NaCl concentrations

indicating the onset destabilization process. Furthermore, the samples precipitated completely after few hours of NaCl addition. Thus, the observation of stable suspension of colloidal Ag-NPs at low NaCl concentrations, despite the drop in zeta potential from − 55.1 to − 3.4 mV, followed by the precipitation of particles at high NaCl concentrations indicated that steric or depletion type of stabilization could be the predominant mechanisms that imparted stability to the Ag-NPs. The drop in the zeta potential could have been attributed to neutralization of electrostatic charges of carboxylic groups of aminoacids, which conferred electrostatic stabilization to Ag-NPs. This was further corroborated by the TEM analysis of samples (lipopeptide concentration = 62.5 mg L^{-1}) (Fig. 12a), which showed that most of the micelles were seen detached from the Ag-NPs, indicative of depletion type of stabilization. However, at low lipopeptide concentration of 25 mg L^{-1}, the close observation of TEM images of particles revealed the presence of a layer of thin film over the Ag-NPs (Fig. 12b).

This encapsulation of Ag-NPs by lipopeptide bilayers indicated that steric/electro static stabilization conferred stability to Ag-NPs at low lipopeptide concentration. At high lipopeptide concentration (125 mg L^{-1}), in addition to micelles, vesicles were also observed which imparted stability predominantly by depletion type of stabilization. On the whole, the stability studies revealed that lipopeptide stabilized the Ag-NPs by more than one mechanism for different initial lipopeptide concentrations. Although all types of stabilization were exhibited by anionic lipopeptides as revealed by TEM analysis, depletion type of stabilization conferred greater stability to Ag-NPs for higher lipopeptide concentrations. However, the major decisive factor, which dictates the concentration to be

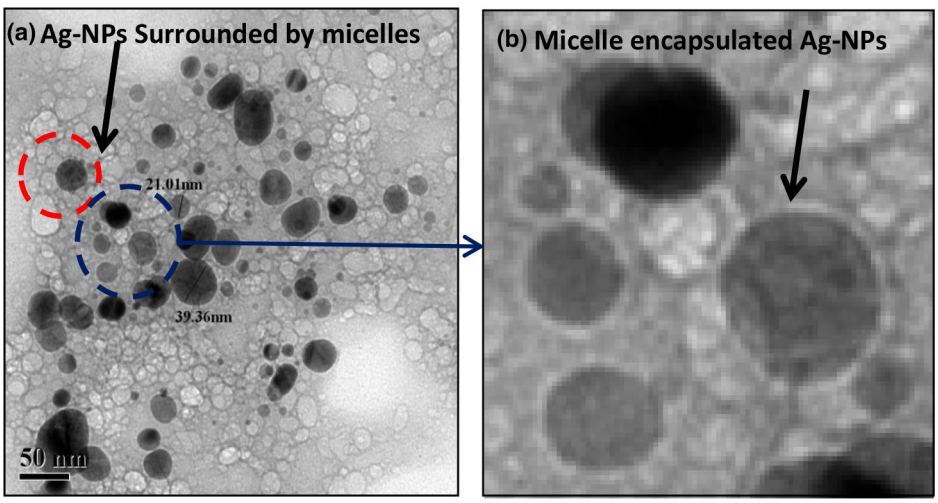

Fig. 12 TEM images of Ag-NPs stabilized by lipopeptides **a** micelles detached from the particles **b** particles encapsulated within a thin bi-layer of lipopeptide (enlarged section of the **a** as indicated in Blue dotted circle)

Table 2 The zone of bacterial inhibition for different Ag-NPs against the tested pathogens

Bacteria	Zone of inhibition (mm)									
	A_1	A_2	A_3	B_1	B_2	B_3	$AgNO_3$	LP	LP + $NaBH_4$	Ag-NaP
Gram-negative *Escherichia coli*	14	12	–	–	–	–	12	10	–	11
Proteus vulgaris	11	11	–	7	8	–	12	10	–	10
Gram-positive *Bacillus subtilis*	20	13	7	–	9	–	15	13	8	13
Micrococcus flavus	11	11	7	7	8	8	12	11	7	10
Serratia marcescens	10	11	–	7	8	7	17	10	8	1.0

A, B → Ag–NaP prepared by method A and B; 1, 2, 3 and 4 → 25, 62.5, 125 and 500 mg/L lipopeptide; (–) did not show any zone of inhibition; LP → lipopeptide; all values are averages of two experiments

used during synthesis is the intended end-application of Ag-NPs.

Antimicrobial studies

Since both lipopeptides and Ag-NPs used in this current work have been extensively studied for their antimicrobial properties, it is important to investigate the antimicrobial activities of the resulting lipopeptide-conjugated Ag-NPs against its free forms, i.e., lipopeptide and naked Ag-NPs. The Ag-NPs synthesized by two methods were tested for their antimicrobial activities (Table 2) against two Gram-negative bacteria, *E. coli* and *Proteus vulgaris*, and three Gram-positive bacteria *Bacillus subtilis, Micrococcus flavus* and *Serratia marcescens*. The zones of inhibition (in cm) of different Ag-NPs samples against the tested bacteria are given in Table 2. The samples of method A with 25 and 62.5 mg L^{-1} of lipopeptide showed bacterial growth inhibition against all the tested bacteria, with maximum (20 mm) against the Gram-positive *Bacillus subtilis*. These values were comparable with that of $AgNO_3$, naked Ag-NPs and lipopeptide separately.

Although, the Ag-NPs of Method B showed narrow size distribution as revealed by TEM, they exhibited comparatively lower antimicrobial activities against test bacteria. The antimicrobial studies of the samples from two methods revealed that the antimicrobial activity of Ag-NPs is dependent both on lipopeptide concentration and the method of synthesis. However, further studies are required to assess for the sustained particle releasing ability of lipopeptide-conjugated Ag-NPs and to assess the synergistic effects of individual lipopeptide and Ag-NPs in lipopeptide-conjugated Ag-NPs against bacteria.

Conclusion

The use of natural surfactants as stabilizing agents has emerged as a green alternative to synthetic surfactants in NP synthesis. Lipopeptides, owing to their metal chelating abilities, can also assist in directing the shape of the NPs during synthesis. In the current study, CFUF-purified lipopeptide was used as capping agent for the single-step synthesis of Ag-NPs. The mean size and the size distribution of the Ag-NPs were found to be strongly dependent on the method of synthesis and the initial lipopeptide concentration. The size of the nanoparticles changed from spherical to varied structures (anisotropic) and increased in size with the increase in anionic lipopeptide concentration. Although the preliminary studies revealed that the lipopeptide at high concentrations acted as templates for the growth of Ag-NPs, further studies are to be conducted to ascertain this feature. Among the two methods adopted, Method A, where in the excess reactant was added to limiting reactant resulted in stable Ag-NPs with zeta potential up to − 55.4 mV for a lipopeptide concentration of 62.5 mg L^{-1}. The stability of the particles was not affected up to the NaCl concentration of 25 g L^{-1}. A combination of steric and depletion stabilization was found to be the predominant mechanisms which stabilized the Ag-NPs. The Ag-NPs were found to be stable for 6 months without any precipitation. Antimicrobial studies revealed that Ag-NPs of method A were found to sensitive against all the bacteria tested.

Compliance with ethical standards

Conflict of interest The authors declare that there is no conflict of interest regarding the publication of this paper.

References

Baruwati B, Polshettiwar V, Varma RS (2009) Glutathione promoted expeditious green synthesis of silver nanoparticles in water using microwaves. Green Chem 11:926–930

Biswas M, Raichur AM (2008) Electrokinetic and rheological properties of nano zirconia in the presence of rhamnolipid biosurfactant. J Am Ceram Soc 91:3197–3201

Chaudhari VR, Haram SK, Kulshreshtha SK, Bellare JR, Hassan PA (2007) Micelle assisted morphological evolution of silver nanoparticles. Colloids Surf A Physicochem Eng Asp 301:475–480

Chen D-H, Hsieh C-H (2002) Synthesis of nickel nanoparticles in aqueous cationic surfactant solutions. J Mat Chem 12:2412–2415

Cushing BL, Kolesnichenko VL, O'Connor CJ (2004) Recent advances in the liquid-phase syntheses of inorganic nanoparticles. Chem Rev 104:3893–3946

Derkacs D, Chen WV, Matheu PM, Lim SH, Yu PKL, Yu ET (2008) Nanoparticle-induced light scattering for improved performance of quantum-well solar cells. Appl Phys Lett.https://doi.org/10.1063/1.2973988

Desai R, Mankad V, Gupta SK, Jha PK (2012) Size distribution of silver nanoparticles: UV–Visible spectroscopic assessment. Nanosci Nanotechnol Lett 4:30–34

Du Y et al (2018) Preparation of versatile yolk-shell nanoparticles with a precious metal yolk and a microporous polymer shell for high-performance catalysts and antibacterial agents. Polymer 137:195–200

Eastoe J, Warne B (1996) Nanoparticle and polymer synthesis in microemulsions. Curr Opin Colloid In 1:800–805

Ewais H (2014) Kinetics and mechanism of the formation of silver nanoparticles by reduction of silver (I) with maltose in the presence of some active surfactants in aqueous medium. Transit Met Chem 39:487–493

Goesmann H, Feldmann C (2010) Nanoparticulate functional materials. Angew Chem Int Ed 49:1362–1395. https://doi.org/10.1002/anie.200903053

Gutiérrez-Wing C, Velázquez-Salazar JJ, José-Yacamán M (2012) Procedures for the synthesis and capping of metal nanoparticles. In: Soloviev M (ed) Nanoparticles in biology and medicine. Methods in molecular biology, vol 906. Humana Press, New York, pp 3–19

Hanh N, Quy OK, Thuy NP, Tung LD, Spinu L (2003) Synthesis of cobalt ferrite nanocrystallites by the forced hydrolysis method and investigation of their magnetic properties. Phys B Condens Matter 327:382–384

Hutter E, Fendler JH, Roy D (2001) Surface plasmon resonance studies of gold and silver nanoparticles linked to gold and silver substrates by 2-aminoethanethiol and 1,6-hexanedithiol. J Phy Chem B 105:11159–11168

Kasture M, Singh S, Patel P, Joy PA, Prabhune AA, Ramana CV, Prasad BLV (2007) Multiutility sophorolipids as nanoparticle capping agents: synthesis of stable and water dispersible co nanoparticles. Langmuir 23:11409–11412

Kiran GS, Sabu A, Selvin J (2010) Synthesis of silver nanoparticles by glycolipid biosurfactant produced from marine Brevibacterium casei MSA19. J Biotechnol 148:221–225

Liao Z, Wang H, Wang X, Wang C, Hu X, Cao X, Chang J (2010) Biocompatible surfactin-stabilized superparamagnetic iron oxide nanoparticles as contrast agents for magnetic resonance imaging. Colloids Surf A Physicochem Eng Asp 370:1–5

Narayanan KB, Sakthivel N (2010) Biological synthesis of metal nanoparticles by microbes. Adv Colloid Interface Sci 156:1–13

Noguez C (2007) Surface plasmons on metal nanoparticles: the influence of shape and physical environment. J Phy Chem C 111:3806–3819

Pattekari P, Zheng Z, Zhang X, Levchenko T, Torchilin V, Lvov Y (2011) Top-down and bottom-up approaches in production of aqueous nanocolloids of low solubility drug paclitaxel. Phys Chem Chem Phys PCCP 13:9014–9019

Raichur AM (2007) Dispersion of colloidal alumina using a rhamnolipid biosurfactant. J Dispers Sci Technol 28:1272–1277

Rangarajan V, Dhanarajan G, Sen R (2014) Improved performance of cross-flow ultrafiltration for the recovery and purification of Ca2 + conditioned lipopeptides in diafiltration mode of operation. J Memb Sci 454:436–443

Rangarajan V, Sen R (2013) An inexpensive strategy for facilitated recovery of metals and fermentation products by foam fractionation process. Colloids Surf B 104:99–106

Rao CNR, Kulkarni GU, Thomas PJ, Edwards PP (2000) Metal nanoparticles and their assemblies. Chem Soc Rev 29:27–35

Raveendran P, Fu J, Wallen SL (2003) Completely "green" synthesis and stabilization of metal nanoparticles. J Am Chem Soc 125:13940–13941

Singh V, Khullar P, Dave PN, Kaura A, Bakshi MS, Kaur G (2014) pH and thermo-responsive tetronic micelles for the synthesis of gold nanoparticles: effect of physiochemical aspects of tetronics. Phys Chem Chem Phys 16:4728–4739

Varade D, Haraguchi K (2012) One-pot synthesis of noble metal nanoparticles and their ordered self-assembly nanostructures. Soft Matter 8:3743–3746

White GV, Kerscher P, Brown RM, Morella JD, McAllister W, Dean D, Kitchens CL (2012) Green synthesis of robust, biocompatible silver nanoparticles using garlic extract. J Nanomater 2012:55–55

Xing X, Sun G, Li Z, Ngai T (2012) Stabilization of colloidal suspensions: competing effects of nanoparticle halos and depletion mechanism. Langmuir 28:16022–16028

Yonezawa T, Onoue S-Y, Kimizuka N (2000) Preparation of highly positively charged silver nanoballs and their stability. Langmuir 16:5218–5220